NUMERICAL AND EXPERIMENTAL ANALYSES OF A VARIABLE BUOYANCY SYSTEM FOR AN AUTONOMOUS UNDERWATER VEHICLE

(DOI No: 10.3940/ijme.2021.a1.647)

B K Tiwari and **R Sharma**, Design and Simulation Laboratory, Department of Ocean Engineering, IIT Madras, India

KEY DATES: Submitted: 18/05/2020, Final acceptance: 10/11/2020, Published: 25/03/2021

SUMMARY

Autonomous Underwater Vehicles (AUVs) are widely used for marine survey, in both the coastal and deep sea areas and they are applicable to both civil and defense applications. They are pre-programmed and can operate without human intervention and this makes them attractive to many marine industries. A concern with AUVs is the high energy consumption required by their thrusters for depth control, buoyancy change and manoeuvrability and that adversely affects their performance and endurance. This paper presents the design and development of novel stand-alone variable buoyancy system for AUVs and investigates its performance through numerical and experimental investigations. The design idea is based upon the Pump Driven Variable Buoyancy System (PDVBS) and uses a hydraulic based method to control the buoyancy. The VBS is integrated into a medium sized AUV of 3 m length and the performance of the vehicle in vertical plane is investigated. The results are presented for a buoyancy change requirement of 5 kg and a diaphragm type positive displacement pump, with a buoyancy change rate of 5 kg/min, is utilized. Depth control performance of the AUV and its hovering capabilities, at a desired depth of 60 m using the Linear Quadratic Regulator (LQR) controller, are analysed in detail. Finally, the results indicate that the designed and developed VBS is effective in changing the buoyancy and controlling the heave velocity. These two features are expected to provide higher endurance and better performance in AUVs involved in rescue/attack operations.

NOMENCLATURE

α_0	=	Non dimensional parameter,
ρ	=	Density of the fluid (kg/m^3),
∇	=	Displaced volume (m^3),
a,b	=	Semi axes of the developed VBS,
$\pm\Delta B$	=	Total change in the buoyancy capacity (kg),
B	=	Buoyant force acting (N),
$b(x)$	=	Diameter of the vehicle along x-axis (m),
C_d	=	Drag coefficient,
$D_{\max}$	=	Maximum diameter of the vehicle (m),
e	=	Eccentricity,
g	=	Gravitational acceleration (m/s^2),
L	=	Length of the AUV (m),
m	=	Mass of the vehicle (kg),
m_a	=	Added mass,
M	=	Pitching moment (N-m),
U	=	Speed of the vehicle (m/s),
w	=	Heave velocity (m/s),
W	=	Weight of the AUV (N),
z_G	=	Center of gravity in z-direction (m), and
Z	=	Vertical forces (N).

1. INTRODUCTION

Exploration of the ocean is an exciting and challenging area of interest for the world community and it is relevant for multiple disciplines, e.g. underwater survey, communication, oil and gas exploration, coastal protection, tourism and recreational, and deep sea mining, etc. On current estimates a significant area of the planet earth occupied by water bodies remains unexplored and unmapped. Ocean exploration can be achieved with surface and underwater vehicles. Surface vehicles are preferred after the preliminary and exploratory surveys have been completed and these are preferred with Underwater Vehicles (UVs). Herein, the focus is on the UVs and they are classified into: Human Occupied Vessels (HOVs) such as submarine used for the defense applications and deep research vessels, and Unmanned Underwater Vehicles (UUVs) such as Remotely Operated Vehicles (ROVs) and Autonomous Underwater Vehicles (AUVs). Out of these UVs, the AUV is widely used for both the civil and defense applications related to survey, mining, launching and recovering of torpedoes, etc. in the ocean environment. AUVs are designed with propellers and/or thrusters and these propellers/thrusters apart from their usages related to propulsion they are highly inefficient for other applications, e.g. depth control, buoyancy change, maneuvering, and hovering, etc. Despite these inefficiencies they are still used and hence the AUV consumes high energy during the operations and this adversely affects its range and endurance.

In this environment, through some of the earlier works (Tiwari et al. (2016), and Tiwari and Sharma (2018, 2020)), it has been shown that the application of Variable Buoyancy System (VBS) in the UVs is effective for minimizing the energy consumption during different operations such as sinking, rising or station keeping at any desired depth without operating the thrusters for AUVs. Similar benefits extend for the Autonomous Underwater Gliders (AUGs), e.g. saw-tooth motion of gliders. Minimization of energy consumption increases the range and endurance of UVs.

1.1 MOTIVATION AND CONTRIBUTION

An early application of the VBS can be found in Seahorse AUV (Dzielski et al., 2002) and it was developed by the ARL, USA. This AUV is very large in size and was designed for the Naval Oceanographic Office (NAVOCEANO) and integrated with the VBS of $\pm\Delta B$ = 90 kg buoyancy capacity.

In similar line, another very large AUV - URASHIMA AUV (Hyakudome et al., 2002) was developed by the JAMSTEC for deep and long cruising ranges, and it was integrated with the buoyancy system of 50 liters of oil transferable capacity to control the buoyancy. In this design oil is transferred from the oil tank to an inflatable/deflatable rubber bladders and vice-versa to change the buoyancy. Bladders are located outside the vehicle and they are known to increase the drag and are difficult to design and operate at deep water depths. An alternative approach existed before and it was implemented in Theseus AUV (Thorleifson et al., 1997). This was developed by the International Submarine Engineering (ISE) and integrated with the buoyancy system of $\pm\Delta B$ = 95 kg, to compensate for the buoyancy change (i.e. decrease in weight) due to laying the underwater fiber optic cables.

Starting since 2000, the concept of the VBS has also found some applications in the AUGs, e.g. Sea glider (Eriksen et al., 2001) and Spray glider (Sherman et al., 2001) are integrated with buoyancy systems and control their buoyancies by changing the displaced volume of the external bladders in the order of around 200 milliliter. In Slocum glider, Douglas et al. (2001) used single-stroke displacement piston pump with rolling diaphragm seal to move certain volume of water and the buoyancy was controlled by changing the overall weight of the glider. Shibuya et al. (2013) and Ranganathan et al. (2017) explored another method to change the buoyancy and it is by changing the displaced volume of metal bellows by either operating the electric linear actuator or using paraffin wax with peltier device method.

1.2 LIMITATIONS OF THE EXISTING RESEARCH

Limitations of the existing research are as follows:

- All the available buoyancy systems for AUVs are very large and they can be installed only in the very large sized AUVs, e.g. beyond 8 m in length. Furthermore, the design process of VBS is neither known fully nor is scalable. Existing researches present the results on VBS in terms of design summaries only and do not report results with verifiable/reproducible details.
- For the AUGs, all the available buoyancy systems cater to very low capacity of buoyancy control and here too neither the design approach nor the detailed implementation and integration of the VBS and AUG are known.

In present work, the focus is on addressing these limitations.

1.3 RESEARCH CONTRIBUTIONS

This paper focuses on the design and development of a novel VBS and present the design approach in-detail. The VBS is conceived in the environment of integration and is capable of performing the following tasks efficiently with low energy consumption:

- Pitch control: Trimming of the vehicle can be achieved using VBS at lower speed of the vehicle when the control surface becomes ineffective to produce sufficient pitching moment to control the pitch angle.
- Rate of change of depth control: Change in the heave speed, both in diving in and diving out modes can be achieved.
- Emergency release of recovery: By changing the difference between the weight and buoyancy emergency release of recovery can be achieved.
- Ability of station keeping in the vertical water column at desired depths can be achieved.
- Ability to compensate for the changes in density of fluid can be achieved.

In this paper the detailed design approach with sufficient technical details that has been used to control the net change in buoyant force and detailed performance analyses of the VBS in the stand alone mode are presented to establish the 'Proof of Concept (PoC)'. Furthermore, the developed VBS is integrated with an AUV of 3 m length to study the performance of UV for different buoyancy capacities.

Remaining of the paper is organized as: Section 2 discusses the design approach and includes mathematical modeling of the VBS in stand-alone mode and numerical and experimental results for performance analysis of the VBS in stand alone mode; Section 3 presents mathematical modeling of the AUV and its integration with the VBS; Section 4 presents the performance analysis of the AUV integrated with developed VBS and Section 5 concludes the paper with some identifications about the future scope of research.

2. DESIGN APPROACH

Following Jensen (2009), the net buoyancy of submerged body/vehicle is defined as:

$$\Delta B = \left(W - B\right)/g = \left(m - \rho\nabla\right) \tag{1}$$

where W is the total weight of vehicle, B is the buoyancy of the vehicle, ∇ is the volume displaced by the vehicle, g is the gravitational acceleration, and ρ is the density of fluid. If the net buoyant force $\Delta B = 0$, then the vehicle is neutrally buoyant, if $\Delta B < 0$ then it is positively buoyant, and if $\Delta B > 0$ then the vehicle is negatively buoyant. So, in order to control the depth, based upon the operational requirements ΔB needs to be changed and this can be done either by changing the mass of the vehicle m or by changing the volume displaced by the vehicle ∇. Different methods to control the ∇ are as follows:

- Hydraulic driven VBS: Here, oil tank and rubber bladder with hydraulic mechanism for fluid transfer in either way are used.
- Pneumatic driven VBS: Here, expansion/contraction of the rubber bladder by high pressure compressed air is used. At every cycle during expansion of the bladder mass of the air from compressed air chamber gets filled in to the bladder and during the contraction volume of the air from bladder gets exhausted to the open environment. This results into reduction of the pressure and mass of air of high pressure chamber in every cycle.
- Using the metal bellow: Expansion/compression of the metal bellows by linear actuator or paraffin wax with peltier device and moving the hollow piston.
- Another method of buoyancy control is by changing the m and it can be achieved by the following means:
- Releasing the dead weight: This implies that only one way buoyancy can be controlled and because of this reason it is suitable for emergency cases only.
- Use of water ballast tank: Water ballast tanks are filled/emptied and through these processes it is easy to control the mass of the vehicle. This approach is suitable for large range of requirements, i.e. low to medium to high desired changes in the buoyancy. Present work focuses on this approach.

2.1 MECHANICAL DESIGN OF THE COMPONENTS OF VBS

Components of the designed and developed VBS include: Hemispherical ballast tank, diaphragm pump, 12 V DC solenoid valve to control the flow direction, flow sensor, check valves, micro controller and data logging system. For product realization and demonstration of PoC, the proposed designed VBS is considered for $\pm\Delta B = 5$ kg buoyancy capacity. It consists of three modular parts as shown in Fig. 1. Fig. 1A shows the hemispherical ballast tank in which water can be filled or from which it is emptied in order to change the buoyancy and its dimensions are: 150 mm inner radius, and 5 mm thickness attached with 7.5 mm thick flange. Fig. 1B shows the cylindrical middle body of 65 mm height to keep all the components such as pump, solenoid valves in the connection, and flow sensor, etc. Fig. 1C shows the upper enclosed dome of the same dimensions as the bottom hemispherical ballast tank.

Material selection for the external body of ballast tank depends upon the requirement of operating depth, i.e. hydrostatic pressure against which the tank should neither break nor buckle and at the same time should offer light weight. Based upon these constraints, herein Epoxy-Fiber Reinforced Plastic (e-FRP) material is considered for the ballast tanks, for more details see Tiwari and Sharma (2020). Polyvinyl Chloride (PVC) material of 10 mm thickness is used for the middle part (Fig. 1B) and that also includes the circular disk attached to the lower side and flange on the upper side.

Additional details of the design parameters of modular components of VBS are listed in Table 1. Table 1A lists the mass of various components of VBS and Table 1B lists the mass of displaced volume for various components of the developed VBS. Fig. 2A shows Computer Aided Design (CAD) model of the complete VBS in which two circular iron rings at the bottom side are fixed with system. Here, it is noted that these circular iron rings are needed to ensure that the VBS has enough contact area to rest on bed (if needed?), has proper stand and shifts the Center of Gravity (CG) of the complete system downward to increase its stability.

These iron rings are not part of the design of VBS *per-se* and if the VBS is not in the stand alone mode then these will not be needed, e.g. when the VBS is used in an AUV. Fig. 2B shows the weighing of the complete VBS. Presented design of VBS is capable of $\pm\Delta B = 5$ kg, but the deadweights of 6.55 kg are added in order to compensate for the excess buoyancy of VBS. In this case the total change in buoyancy capacity remains same but $+\Delta B$ gets reduced to 1.5 kg and $-\Delta B$ rise to 3.5 kg. The VBS will be neutrally buoyant when 1.5 kg water is added to the ballast tank. Furthermore, to achieve equally positive and negative buoyancy capacities of the VBS, the deadweight can be reduced by 1 kg.

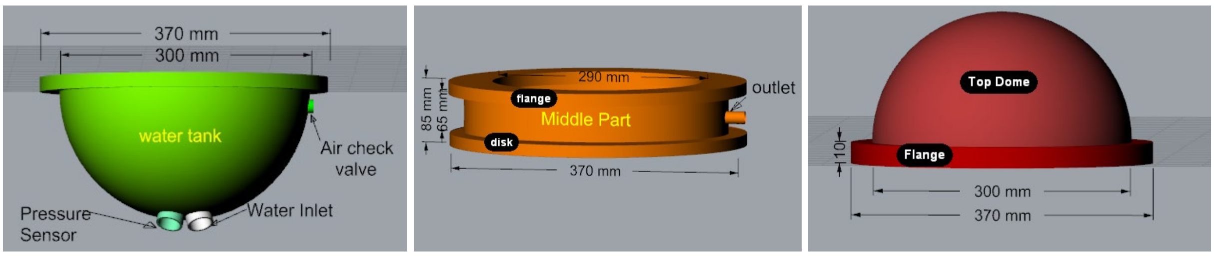

(A) (B) (C)

Figure 1: Modular design of the complete VBS: (A) Ballast tank, (B) Middle body and (C) Upper enclosed dome.

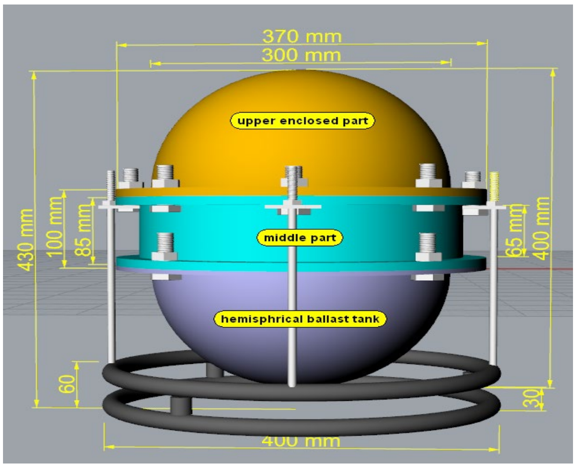

Figure 2: A - A CAD model of the VBS.

Figure 2: B - Weighing of the complete VBS.

Table 1A: List of mass of the VBS components.

S. No.	Components considered	Value (kg)
1	Upper dome	2.00
2	Middle part +Bottom ballast tank	6.45
3	Mass of pump, solenoid valve, flow sensor, connecting tubes etc.	3.85
4	Mass of the bottom two circular and four vertical rods	6.30
5	Mass of the dead weight used	6.55
6	Total mass	25.15

Table 1B: List of mass of displaced volume for all the components of VBS.

S. No.	Component-wise Volume displaced	Volume displaced (cm^3)	Mass of the displaced Volume (kg)
1	Upper dome (V_t)	9000	9.2250
2	Middle part (V_{mi})	7100	7.2770
3	Ballast tank (V_{bot})	9000	9.2250
4	Circular ring (V_{cr})	750	0.7680
5	Vertical ring (V_{vr})	68	0.0697
6	Total	26000	26.650

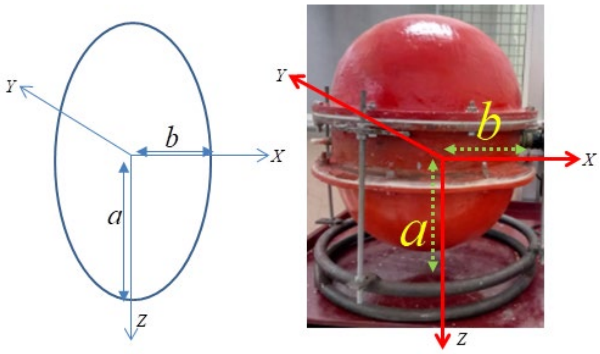

Figure 3: A - Approximation of the designed VBS to prolate ellipsoid shape.

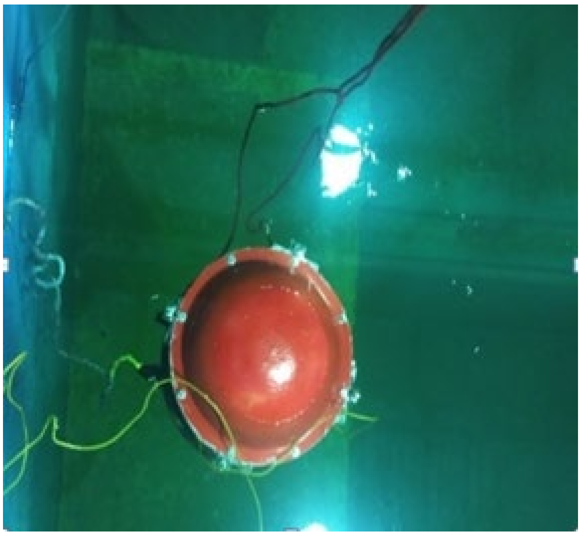

Figure 3: B - Leakage and stability testing of the VBS in the stand-alone mode.

As shown earlier, Fig. 3B shows the leakage and stability testing of the developed VBS. Using the numerical simulations, Fig. 6A indicates the variation of heave velocity and depth of VBS both in sinking and rising conditions. Fig. 6B shows the comparison of experimental and simulation results for depth of VBS in the stand-alone mode for both the sinking and rising. Details about the experiments and comparison are reported in Appendix A.

To ensure that the results are verifiable and open to critical scrutiny the video of experimental can be accessed at: **VBS_testing** (website: www.youtube.com/watch?v=8bt0BszMqwE&feature=youtu.be).

2.2 MATHEMATICAL MODELING OF THE VBS IN STAND-ALONE MODE

A mathematical model is developed for the VBS in stand-alone mode to study its performance and the focus is only in one direction, i.e. vertically up/down. Now, the force balance equation can be written as follows:

$$m\dot{w} = F_G - F_B - F_a - F_D + \Delta W \text{ , and} \tag{2}$$

$$m\dot{w} = mg - \rho V_{di} g - m_a \dot{w} - \frac{1}{2} C_D \rho A_p |w| w + \Delta W \tag{3}$$

where m is the mass of system, ΔW is the change in weight of the system, F_G is the gravitational force, F_B is the buoyant force, F_D is the drag force, g is the gravitational acceleration, ρ is the fluid density , V_{di} is the displaced volume by the system, C_D is the drag coefficient, w is the velocity in vertical plane (i.e. heave velocity), m_a is the added mass and $\dot{w}$ is the acceleration of vehicle in the vertical plane. For the neutrally buoyant condition, i.e. when $mg = \rho V_{di} g$, Equation (3) gets reduced to the following:

$$(m + m_a)\dot{w} = \Delta W - \frac{1}{2} C_D \rho A_p |w| w, \tag{4}$$

$$\dot{w} = \frac{(-1/2 \bullet C_D \rho A_p |w| w)}{(m + m_a)} + \frac{\Delta W}{(m + m_a)}, \text{ and} \tag{5}$$

$$\dot{z} = w \tag{6}$$

where m_a is computed based on the assumption made for the designed VBS as of prolate ellipsoid shape (shown in Fig. 3A). Following, Fossen (2011) the added mass (m_a) for prolate ellipsoid can be computed as follows:

$$m_a = \left(\frac{-\alpha_0}{2 - \alpha_0}\right) m \text{, and} \tag{7}$$

$$\alpha_0 = \frac{2(1-e^2)}{e^3}\left[0.5 \ln\left(\frac{1+e}{1-e}\right) - e\right], \text{ and } e = 1 - \left(\frac{b}{a}\right)^2 \tag{8}$$

where α_0 is a non-dimensional parameter, e is the eccentricity, a and b are the semi-axes of prolate ellipsoid.

2.3 NUMERICAL AND EXPERIMENTAL RESULTS FOR PERFORMANCE ANALYSIS OF THE VBS IN STAND ALONE MODE

Numerical simulation parameters of the VBS in stand-alone mode are listed in Table 2 and Fig. 4 shows all the internal connection of various components (i.e. pump, flow sensor, power supply, and solenoid valve for the buoyancy system, etc.).Considering the open conditions, simulation results for VBS in the stand alone mode are shown in Fig. 5.

Fig. 5A indicates the variation of heave/terminal velocity versus the time and the results are presented for 1.5 kg, 2.0 kg and 2.5 kg of negative buoyancy changes. Again, for the open loop condition, Fig. 5B indicates the variation of depth versus time of VBS in the stand alone mode. These variations are expected because higher negative buoyancy (weight > buoyancy) will result into higher heave/terminal velocity and it can noted that the depth is linearly increasing with time. Higher heave/terminal velocities (linear depth resulting into constant velocity at zero acceleration) are preferred in the design of UVs for defense applications related to rescue and attack operations.

Overall, it can be observed that the simulation results indicate desirable performances for different buoyancy capacities. In the experimental testing, high sinking speed requires high depth to be available in the water tank or water body.

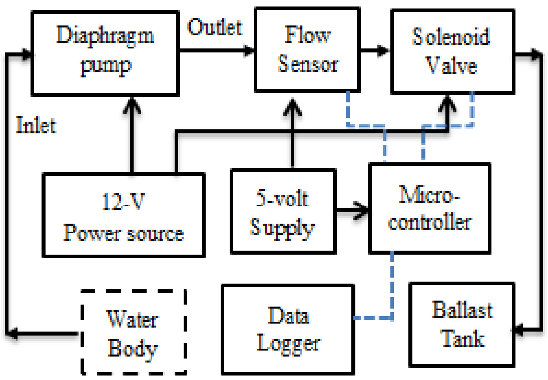

Figure 4: Details of the internal connections of various components.

In the present work, experimental tests were conducted in the water tank and the available depth is limited to only 2 - 3 m and because of these limitations only 0.5 kg of buoyancy change is considered for the experimental testing.

Table 2: List of the numerical simulation parameters of the VBS in stand-alone mode.

S. No.	Parameters	Value
1	Mass (m) (neutrally buoyant condition)	26.65 kg
2	Drag coefficient (C_D)	0.8
3	Density (ρ)	1025 kg/m^3
4	Added mass (m_a)	11.72 kg

This video has been put on ‘youtube’ to ensure that the results are available for a larger group of audiences for critical scrutiny and review. From this video clearly it can be observed that the developed VBS in the standalone mode starts with a positive buoyant condition and then as the water is filled inside the ballast tank, the system becomes negatively buoyant. In the negative buoyant condition, the weight is higher than the buoyancy and so the VBS will start sinking. This is clearly seen in the video.

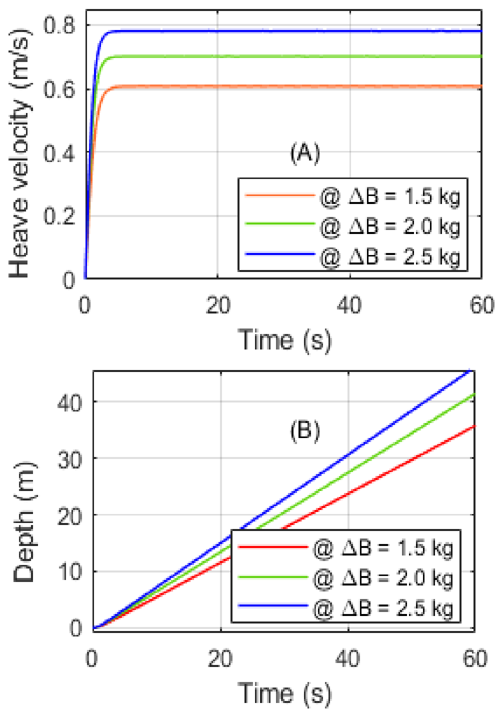

Figure 5: A - Open loop simulation results of the heave velocity variation versus time, and B - Depth variation versus time of the VBS in stand-alone mode.

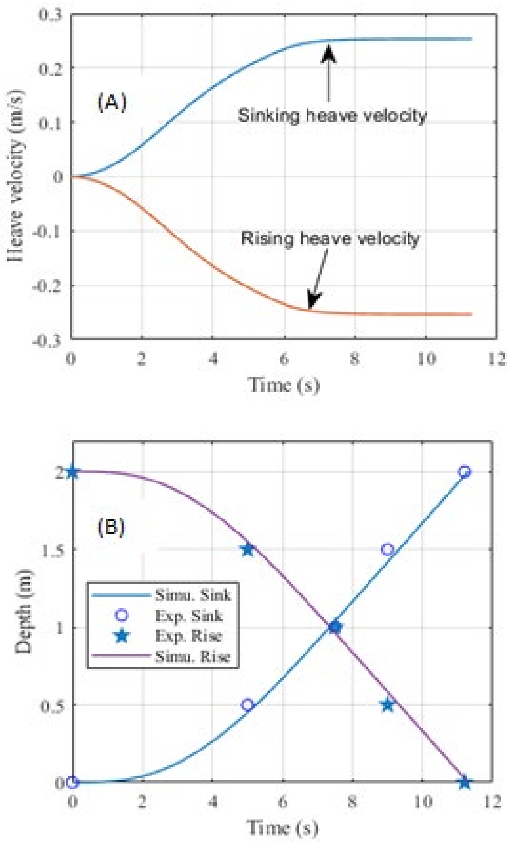

Figure 6: A-Variation of the heave velocity versus time, and B- comparison of experimental and simulation results for depth of VBS in the stand-alone mode for both the sinking and rising.

Later, after reaching the desired (pre-selected depending upon the constraints of water inside the Deep Water Flume (DWF)) depth of 2.0 m, as water from the ballast tank is removed to the external environment, the weight starts reducing and as the buoyancy will remain the same, the B - W becomes positive. This makes the VBS to come up or rise back to the surface.

2.4 OPERATIONAL MODE OF VBS MODEL FOR TRIM/DEPTH CONTROL OF UV

Buoyancy control process model is shown in Fig. 7 and it indicates both the force and moment generated by the VBS while in operation. In these operations the pressure sensors sends the signal for the requirement of increase or decrease in the buoyancy in order to control the depth of operation and Inertial Measuring Unit (IMU) sensor for attitude/pitch control of the vehicle.

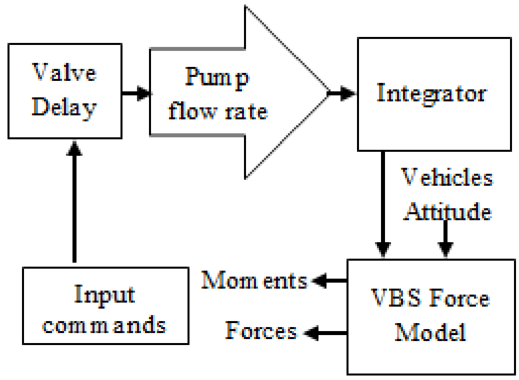

Figure 7: Buoyancy control process model indicating the force or moment generated by the VBS while in operation.

After some time delay (in present work 500 ms has been considered) of valve and operating the pump at any specific flow rate; integrating the flow rate for specified time interval results into the desired amount of buoyancy change. This gets transferred into change of the buoyant force and also the moment about the CG of the vehicle in order to control the vertical motion as well as the attitude or trimming of the vehicle. It is important to note here that the generation of moment is related to the difference and change in CG of the vehicle from the origin of the vehicle.

3. MATHEMATICAL MODELING OF THE AUV INTEGRATED WITH VBS

In this section a novel VBS is presented, which is capable of important applications: Operations in the stand alone mode applicable for ocean/sea buoys; and Operations in the integrated mode applicable to all the UVs. Herein, it can be noted that the applications can cover all the other UVs also but because of the restrictions of space, focus is only on the AUV.

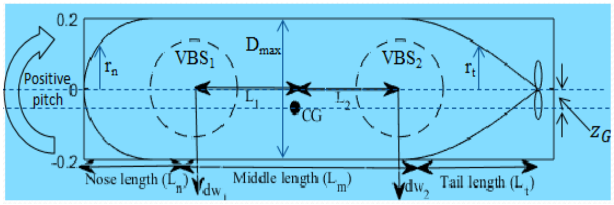

Figure 8: Geometrical shape of the AUV integrated with VBS.

Geometrical shape of the AUV which is integrated with two VBS is shown in Fig 8. First VBS is at the nose side at distance of L_1 and second is at distance of L_2 from the CG of the vehicle. Buoyancy capacity is $\pm\Delta B$ = 5 kg for each of the VBSs and both of them are integrated with the AUV. Detailed analysis of the AUV is done to achieve desired depth of 60 m and hover at the same without operating the propeller. In reference to Fig. 8, geometric details are as follows:

$$r_n = \frac{D_{\max}}{2}\left\{1-\left(\frac{L_n - x}{L_n}\right)^{n_n}\right\}^{1/n_n} ;\, for\ 0 \le x < L_n, \tag{9}$$

$$r_m = \frac{D_{\max}}{2};\quad for\ L_n \le x \le (L_n + L_m), \text{ and} \tag{10}$$

$$r_t = \frac{D_{\max}}{2}\left\{1-\left(\frac{x - L_n - L_m}{L_t}\right)^{n_t}\right\};(L_n + L_m) < x \le L \tag{11}$$

where r_n, r_t, n_n, n_t $D_{\max}$, L_n, L_m,L_t are the nose radius, tail radius, nose shape coefficient, tail shape coefficient, maximum diameter, nose length, tail length and middle length of the AUV respectively. Herein, length of the vehicle is considered 3.0 m to study performance of the AUV integrated with VBS. Mathematical modeling is divided into two parts: Kinematics and Dynamics of the AUV.

3.1 KINEMATICS OF THE AUV

Following Fossen (1994) the kinematic equation of motion in the six Degrees of Freedom (DoF) of an underwater vehicle is written in the body fixed frame as follows:

$$\begin{pmatrix} \dot{\eta}_1 \\ \dot{\eta}_2 \end{pmatrix} = \begin{pmatrix} J_1(\eta_2) & 0 \\ 0 & J_2(\eta_2) \end{pmatrix}\begin{pmatrix} v_1 \\ v_2 \end{pmatrix} \tag{12}$$

where $\eta_1 = [x, y, z]$ and $\eta_2 = [\phi, \theta, \psi]$ are the linear and angular position vectors in earth fixed frame, and $v_1 = [u, v, w]$ and $v_2 = [p, q, r]$ are the linear and angular velocity vectors in the body fixed frame, respectively. The $J_1(\eta_2)$, $J_2(\eta_2)$ are the rotational (transformation) matrices in which $J_1(\eta_2)$ is skew-symmetric matrix. For analyzing the performance of the AUV integrated with VBS, it is noted that the buoyancy system influences the motion of the vehicle in vertical plane only. This is the restriction and it is utilized to simplify the formulations. Now, with this restriction, the kinematic equation of the AUV is as follows:

$$\dot{\theta} = q\cos\phi - r\sin\phi \text{, and} \tag{13}$$

$$\dot{z} = -u\sin\theta + w\cos\theta \tag{14}$$

where θ is the pitch angle, ϕ is the roll angle, q is the pitch rate, $\dot{z}$ is the rate of depth change, r is the yaw rate, u is the surge velocity and w is the heave velocity.

3.2 DYNAMICS OF THE AUV

As mentioned in Section 3.1, influence of buoyancy system to the motion of the vehicle is restricted in the vertical plane only and with this the dynamic equation for the force in z-direction and moment of the vehicle about the y-axis with the notation as defined in SNAME (1950) can be written as follows:

$$\begin{aligned} Z = m(\dot{w} - uq + vr - z_G\left(p^2 + q^2\right) \\ + x_G\left(pr - \dot{q}\right) + y_G(qr + \dot{p})) \end{aligned} \tag{15}$$

$$\begin{aligned} M &= I_y\dot{q} - \left(I_z - I_x\right)rp + I_{yz}\left(pq - \dot{r}\right) - I_{zx}\left(r^2 - p^2\right) \\ &+ m\left[z_G\left(\dot{u} - vr + wq\right) - x_G\left(\dot{w} + vp - uq\right)\right] \end{aligned} \tag{16}$$

where m is mass of the vehicle; v is the sway velocity; p is the roll rate; (x_G, y_G and z_G) is the distance of the CG from origin of the vehicle in x, y and z direction respectively; I_x, I_y and I_z is the mass moment of inertia about x, y and z direction respectively; (I_{zx} and I_{yz}) are the product inertias and all other parameters are same as defined before.

Condition of restricted motion of the vehicle in vertical plane means that the sway velocity $v = 0$, yaw rate $r = 0$, $\dot{u} = 0$ and $x_G = 0$. Additionally, neglecting the non-linear terms, reduces Equations (15) and (16) to the following:

$$\begin{aligned} Z &= m(\dot{w} - uq - x_G\dot{q}) \\ M &= I_y\dot{q} - mx_G(\dot{w} - uq) \end{aligned} \tag{17}$$

where Z is the inertial force in vertical direction, M is the moment about y-axis and other parameters are same as defined before. External forces acting on the vehicle consists of hydrodynamic force, drag force, gravity force, propeller force, and force due to rudder deflection, etc. Herein, propeller force is neglected and assuming that the vehicle is at very low speed, the rudder also becomes ineffective.

Now, the remaining external forces can be written as follows:

$$\begin{aligned}\sum Z =& Z_q{}'' Uq + Z_{\dot{q}}{}'' \dot{q} + Z_w{}'' Uw + Z_{\dot{w}}{}'' \dot{w} + (W - B)\cos\theta \\ & -0.5\rho \int_{nose}^{tail} C_D b(x)(w - xq)\left|w - xq\right| dx + (dw_1 + dw_2)\cos\theta\end{aligned} \quad (18)$$

where $\sum Z$ is the sum of all external forces acting on the vehicle in vertical plane; $Z_q{}'', Z_{\dot{q}}{}'', Z_w{}'', Z_{\dot{w}}{}''$ are the non-dimensional hydrodynamic coefficients; $\dot{q}, \dot{w}$ are the rate of change of pitch and heave velocities, respectively; C_D is the drag coefficient; $b(x)$ is the diameter of the vehicle along the x-axis; and dw_1, dw_2 are the weight of added ballast water to tanks 1 and 2 respectively. Moment acting in vertical plane due to external forces is the following:

$$\begin{aligned}\sum M =& 0.5\rho \int_{nose}^{tail} C_D b(x)(w - xq)\left|w - xq\right| x dx + M_q{}'' Uq \\ & + M_{\dot{q}}{}'' \dot{q} + M_w{}'' Uw + M_{\dot{w}}{}'' \dot{w} + (x_G W - x_B B)\cos\theta \\ & -(z_G W - z_B B)\sin\theta + (-L_1 dw_1 + L_2 dw_2)\cos\theta\end{aligned} \quad (19)$$

where L_1, L_2 are the distances of CG of the VBS_1 and VBS_2 from CG of the vehicle respectively; and x_G, x_B, z_G, z_B are the distances between the CG and CB of the vehicle along the x and z axis from origin of the vehicle respectively. Furthermore, $M_{\dot{q}}{}'', M_w{}'', M_{\dot{w}}{}''$ are the non-dimensional hydrodynamic parameters acting during pitching of the vehicle and other parameters are same as were defined before. These hydrodynamic parameters can be computed either experimentally (i.e. through the Planar Motion Mechanism (PMM) test or maneuvering tests, etc.) or numerically (i.e. using the CFD or strip theory etc.). Herein, the hydrodynamic parameters are used from (Beyazay, 1999) in non-dimensionalized form and these are defined as follows:

$$\begin{aligned}& Z_{\dot{q}}' = -0.00253, Z_{\dot{w}}' = -0.0934, Z_q' = -0.0701, \\ & Z_w' = -0.7844, M_{\dot{q}}' = -0.00625, M_{\dot{w}}' = Z_{\dot{q}}', \quad . \\ & M_q' = -0.0153 \text{ and } M_w' = 0.0512\end{aligned} \quad (20)$$

After mathematical modeling of the AUV integrated with VBS, numerical simulation has been performed to analyze the performance of the 3.0 m length AUV integrated with the developed VBS.

3.3 CONTROLLER DESIGN

In this study, LQR controller is used and tuned properly to control the buoyancy and the rate of change of buoyancy. The application of this controller results into control of the heave velocity and pitch/trim of the vehicle. For these there are two inputs: One from each of the VBS. These result into problem of Multiple Input and Multiple Output (MIMO) and since the LQR controller is suitable for the MIMO problems, therefore it is used in this work, for more details see Katsuhiko et al. (2013). Now, following Stephen et al. (1991) and Katsuhiko et al. (2013), a continuous time based linear system is defined as follows:

$$\dot{\boldsymbol{x}} = \boldsymbol{A}\,\boldsymbol{x} + \boldsymbol{B}\,\boldsymbol{u_{in}} \quad (21)$$

where $\boldsymbol{A}$ is the state matrix, $\boldsymbol{B}$ is the input matrix, $\boldsymbol{x}$ is the state vector, and $\boldsymbol{u_{in}}$ is the input vector. In this the objective is to design the state-feedback controller: $\boldsymbol{u_{in}} = -\boldsymbol{K_c}\,\boldsymbol{x}$ where $\boldsymbol{K_c}$ is the optimal feedback control gain matrix and this minimizes the quadratic cost function $\boldsymbol{J}$ which is defined as follows:

$$\boldsymbol{J}(\boldsymbol{x}, \boldsymbol{u_{in}}) = \int_0^\infty \left(\boldsymbol{x^T Q\, x} + \boldsymbol{u_{in}}^{\boldsymbol{T}} \boldsymbol{R\, u_{in}}\right) dt \quad (22)$$

where $\boldsymbol{Q} \in \mathbb{R}^{n \times n}$ is the positive-definite state weighing matrix and $\boldsymbol{R} \in \mathbb{R}^{n \times n}$ is the positive definite energy weighing matrix which determines the relative importance of the state error and expenditure of the energy, respectively.

Now, to derive an optimal controller gain ($\boldsymbol{K_c}$) which minimizes quadratic cost function, using $\boldsymbol{u_{in}} = -\boldsymbol{K_c}\,\boldsymbol{x}$ in Equation (22) and this reduces in to the following:

$$\boldsymbol{J}(\boldsymbol{x}, \boldsymbol{u_{in}}) = \int_0^\infty \boldsymbol{x}^T \left(\boldsymbol{Q} + \boldsymbol{K_c}^T \boldsymbol{R K_c}\right) \boldsymbol{x} dt \quad (23)$$

where all the parameters are same as defined before and other assumption is as follows:

$$\boldsymbol{x}^T \left(\boldsymbol{Q} + \boldsymbol{K_c}^T \boldsymbol{R K_c}\right) \boldsymbol{x} = -\frac{d}{dt}\left(\boldsymbol{x}^T \boldsymbol{S x}\right) \quad (24)$$

where $\boldsymbol{S}$ is the positive definite symmetric matrix. By differentiating the RHS of Equation (24), it reduces to the following:

$$\begin{aligned}\boldsymbol{x}^T \left(\boldsymbol{Q} + \boldsymbol{K_c}^T \boldsymbol{R K_c}\right) \boldsymbol{x} &= -\dot{\boldsymbol{x}}^T \boldsymbol{S x} - \boldsymbol{x}^T \boldsymbol{S} \dot{\boldsymbol{x}} \\ &= -\boldsymbol{x}^T \left[\left(\boldsymbol{A} - \boldsymbol{B K_c}\right)^T \boldsymbol{S} + \boldsymbol{S}\left(\boldsymbol{A} - \boldsymbol{B K_c}\right)\right] \boldsymbol{x}\end{aligned} \quad (25)$$

where all the parameters are same as defined before and after comparing both the sides of Equation (25), following can be noted:

$$\left(\boldsymbol{A} - \boldsymbol{B K_c}\right)^T \boldsymbol{S} + \boldsymbol{S}\left(\boldsymbol{A} - \boldsymbol{B K_c}\right) = -\left(\boldsymbol{Q} + \boldsymbol{K_c}^T \boldsymbol{R K_c}\right). \quad (26)$$

The performance index $\boldsymbol{J}$ can be computed as follows:

$$\boldsymbol{J} = \int_0^\infty \boldsymbol{x}^T \left(\boldsymbol{Q} + \boldsymbol{K_c}^T \boldsymbol{R K_c}\right) \boldsymbol{x}\, dt\,. \quad (27)$$

From Equations (24) and (27), following can be noted:

$$\begin{aligned} \boldsymbol{J} &= -\boldsymbol{x}^T \boldsymbol{S}\boldsymbol{x} \big|_0^\infty \\ &= -\boldsymbol{x}^T(\infty)\boldsymbol{S}\boldsymbol{x}(\infty) + \boldsymbol{x}^T(0)\boldsymbol{S}\boldsymbol{x}(0) \end{aligned} . \tag{28}$$

All the eigenvalues of $(\boldsymbol{A}-\boldsymbol{B}\boldsymbol{K}_c)$ are assumed to be of negative real part in order to fulfill the system stability criteria and this implies: $\boldsymbol{x}(\infty) \to 0$. With this Equation (28) reduces to the following:

$$\boldsymbol{J} = \boldsymbol{x}^T(0)\boldsymbol{S}\boldsymbol{x}(0) . \tag{29}$$

So from Equation (29) it is concluded that the performance index can be obtained in terms of initial conditions and from Equation (26) following can be noted:

$$\begin{aligned} &(\boldsymbol{A}-\boldsymbol{B}\boldsymbol{K}_c)^T \boldsymbol{S} + \boldsymbol{S}(\boldsymbol{A}-\boldsymbol{B}\boldsymbol{K}_c) \\ &\qquad + \boldsymbol{Q} + \boldsymbol{K}_c^T \boldsymbol{R}\boldsymbol{K}_c = 0 \end{aligned} . \tag{30}$$

Since the $\boldsymbol{Q}$ and $\boldsymbol{R}$ are positive definite symmetric matrices, they can be reduced as follows:

$$\begin{aligned} &(\boldsymbol{A}^T - \boldsymbol{K}_c^T \boldsymbol{B}^T)\boldsymbol{S} + \boldsymbol{S}(\boldsymbol{A}-\boldsymbol{B}\boldsymbol{K}_c) \\ &\qquad + \boldsymbol{Q} + \boldsymbol{K}_c^T \boldsymbol{R}\boldsymbol{K}_c = 0 \end{aligned} . \tag{31}$$

Assuming the $\boldsymbol{R} = \boldsymbol{T}^T\boldsymbol{T}$, following can be noted:

$$\boldsymbol{A}^T\boldsymbol{S} + \boldsymbol{S}\boldsymbol{A} - \boldsymbol{K}_c^T\boldsymbol{B}^T\boldsymbol{S} - \boldsymbol{S}\boldsymbol{B}\boldsymbol{K}_c + \boldsymbol{K}_c^T\boldsymbol{T}^T\boldsymbol{T}\boldsymbol{K} + \boldsymbol{Q} = 0 \tag{32}$$

and this can be written as follows:

$$\begin{aligned} &\boldsymbol{A}^T\boldsymbol{S} + \left[\boldsymbol{T}\boldsymbol{K}_c - (\boldsymbol{T}^T)^{-1}\boldsymbol{B}^T\boldsymbol{S}\right]^T \left[\boldsymbol{T}\boldsymbol{K}_c - (\boldsymbol{T}^T)^{-1}\boldsymbol{B}^T\boldsymbol{S}\right] \\ &\qquad + \boldsymbol{S}\boldsymbol{A} - \boldsymbol{S}\boldsymbol{B}\boldsymbol{R}^{-1}\boldsymbol{B}^T\boldsymbol{S} + \boldsymbol{Q} = 0 \end{aligned} . \tag{33}$$

Following Equation (33), in order to minimize the performance index $\boldsymbol{J}$ with respect to $\boldsymbol{K}_c$, it is required to minimize the following:

$$\boldsymbol{x}^T\left[\boldsymbol{T}\boldsymbol{K}_c - (\boldsymbol{T}^T)^{-1}\boldsymbol{B}^T\boldsymbol{S}\right]^T \left[\boldsymbol{T}\boldsymbol{K}_c - (\boldsymbol{T}^T)^{-1}\boldsymbol{B}^T\boldsymbol{S}\right]\boldsymbol{x} \tag{34A}$$

with respect to the $\boldsymbol{K}_c$. Furthermore, it is noted that the expression is non-negative and the minimum will be zero. This is possible only with the following:

$$\boldsymbol{T}\boldsymbol{K}_c = (\boldsymbol{T}^T)^{-1}\boldsymbol{B}^T\boldsymbol{S} \text{ and} \tag{34B}$$

which results in to the following:

$$\boldsymbol{K}_c = (\boldsymbol{T}\boldsymbol{T}^T)^{-1}\boldsymbol{B}^T\boldsymbol{S} = \boldsymbol{R}^{-1}\boldsymbol{B}^T\boldsymbol{S} . \tag{35}$$

Equation (35) results in to the optimal control gain matrix and the optimal control law for LQR controller. This minimizes the performance index written as follows:

$$\boldsymbol{u}_{in}(t) = -\boldsymbol{K}_c\boldsymbol{x}(t) = -\boldsymbol{R}^{-1}\boldsymbol{B}^T\boldsymbol{S}\,\boldsymbol{x}(t) \tag{36}$$

and the matrix $\boldsymbol{S}$ in the Equation (36) can be computed by solving the Matrix Algebraic Riccatti Equation (MARE) given as follows:

$$\boldsymbol{A}^T\boldsymbol{S} + \boldsymbol{S}\boldsymbol{A} - \boldsymbol{S}\boldsymbol{B}\boldsymbol{R}^{-1}\boldsymbol{B}^T\boldsymbol{S} + \boldsymbol{Q} = 0 . \tag{37}$$

An alternate method to compute the optimal feedback control gain matrix $\boldsymbol{K}_c$ is by using the $lqr(\boldsymbol{A},\boldsymbol{B},\boldsymbol{Q},\boldsymbol{R})$ command in Matlab*™ and herein the same is used. In the present work, initial values of $\boldsymbol{Q}$ and $\boldsymbol{R}$ are $eye(6)\cdot 10^3$ and $eye(2)\cdot 10^2$ respectively, where $eye(6)$ is a 6 by 6 and $eye(2)$ is a 2 by 2 identity matrix. Finally the tuned values are as follows:

$$\boldsymbol{Q} = \begin{bmatrix} 2 & 0 & 0 & 0 & 0 & 0 \\ 0 & 3 & 0 & 0 & 0 & 0 \\ 0 & 0 & 1 & 0 & 0 & 0 \\ 0 & 0 & 0 & 1 & 0 & 0 \\ 0 & 0 & 0 & 0 & 0.9 & 0 \\ 0 & 0 & 0 & 0 & 0 & 0.9 \end{bmatrix} .10^3 \text{ and } \boldsymbol{R} = \begin{bmatrix} 60 & 0 \\ 0 & 60 \end{bmatrix} \tag{38}$$

4. PERFORMANCE ANALYSIS OF THE AUV INTEGRATED WITH DEVELOPED VBS

4.1 OPEN LOOP OPERATIONS

Herein, performance of VBS integrated with an AUV of 3.0 m length is analyzed. First results for the open loop condition are presented. Zero reference in all the simulation results means that the vehicle is neutrally buoyant - half-filled ballast tanks. Fig. 9A indicates the variation of weight addition to ballast tanks versus the time for 1.5, 2.0 and 2.5 kg change of buoyancy at the rate of 5 kg/min. From Fig. 9B it can be clearly observed that 2.5 kg mass is added to the ballast tank in 30 sec and 1.5 kg in 18 s respectively.

However, in the open loop operation once the ballast tanks are completely filled, vehicle starts sinking at constant/terminal velocity. This is shown in Fig. 10A. In Fig. 10A the results are reported for all the three cases of buoyancy additions and from that it can be observed that the achieved sinking speeds are 0.2, 0.23 and 0.27 m/s and these are related to 1.5, 2.0 and 2.5 kg change of buoyancy respectively.

Variation of the depth versus time is plotted in Fig. 10B and from which it can be observed that the depth is continuously increasing with the time and at any point of time the vehicle with 2.5 kg buoyancy change achieves the higher depth than the change in buoyancy of 1.5 kg and 2.0 kg. For the sake of clarity, zoomed parts of variations of the heave velocity and depth of operation versus time for the open loop condition is shown in Fig. 11A and 11B, respectively.

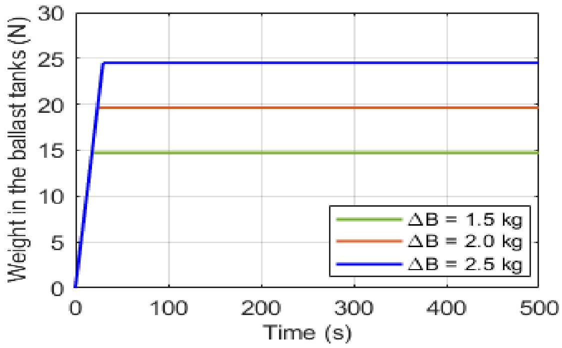

Figure 9: A - Variation of the weight addition in ballast tanks versus time for the open loop operation.

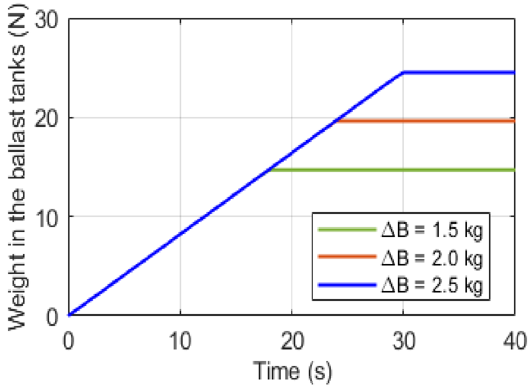

Figure 9: B - Zoomed part of the weight addition in ballast tanks versus time for the open loop operation.

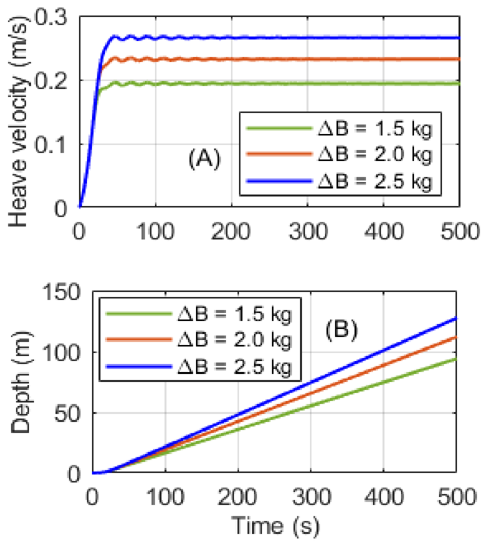

Figure 10: A - Variation of the heave velocity versus time and B - Variation of the depth of operation versus time for open loop condition.

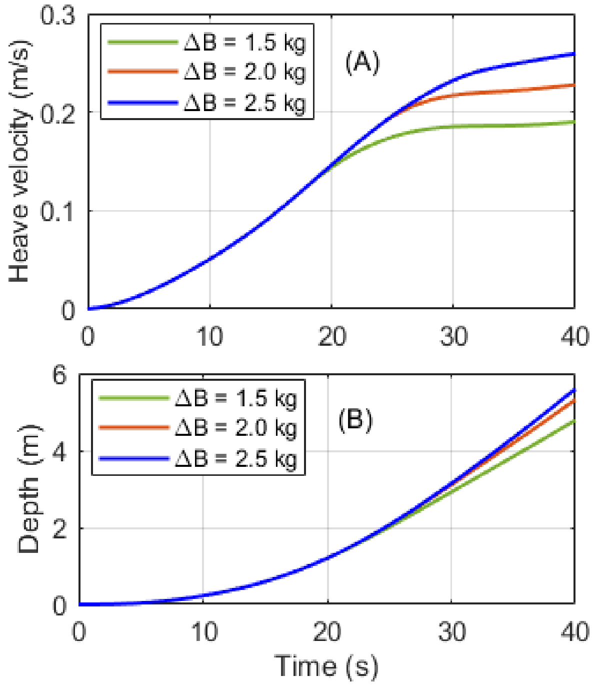

Figure 11: A - Zoom part of the variation of heave velocity versus time and B - Variation of the depth of operation versus time for open loop condition.

From Fig. 11A and 11B it is observed that until the ballast tanks are completely filled and the heave velocity reaches to its maximum, the depth varies non-linearly with time and after that the depth varies linearly with time. These results are along the expected lines and showcase an impressive performance of the proposed design.

4.2 CLOSED LOOP OPERATION

Basic schematic of the closed loop controller is shown in Fig. 12. In actual simulation analysis the numerical values of $\boldsymbol{Q}$ and $\boldsymbol{R}$ (tuning parameters) are used to compute the optimal feedback control gain matrix and initial values of that are chosen randomly. Then they are tuned for the estimation of optimal control gain ($\boldsymbol{K}_c$) matrix for the best performance. Finally the tuned values of $\boldsymbol{Q}$ and $\boldsymbol{R}$ have been already listed through Equation (38) in Section 3.3.

Herein, it is noted that the developed VBS is capable of operating at higher depths at the conceptual design level. But because of the use of positive displacement diaphragm pump limited to operate only up to 6.5 bar (i.e. 65 m depth) pressure, in this study for analyzing the performance of AUV in closed loop operation integrated with the designed VBS of different buoyancy capacities to control, the depth of operation is restricted to 60 m only.

Fig. 13A plots the variation of heave velocity versus time and 13B plots the variation of depth of operation versus time in closed loop operation for three different buoyancy capacities, 1.5, 2.0 and 2.5 kg, respectively. From these results it can be observed that the maximum sinking speed (i.e. terminal velocity) is achieved for 2.5 kg change of buoyancy and minimum sinking speed is achieved for 1.5 kg change of buoyancy.

This is expected because the terminal velocity depends upon the difference of W - B and the higher difference implies higher terminal velocity.

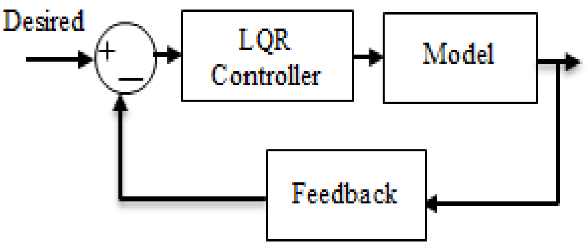

Figure 12: Basic schematic of the closed loop controller.

As the vehicle approaches desired depth of operation, the weight of water inside the ballast tank starts reducing and finally reaches to zero, i.e. half-filled and neutrally buoyant condition. Depth control for the station keeping of AUV at 65 m is achieved with little 1.5 m overshoot in around 500 s and it reaches the desired depth with zero steady state error after 800 s and zero overshoot. These results are highly meaningful because they clearly indicate that the controller performance is good and the desired depth of operation is achieved with negligible oscillations and overshoots.

These features are highly desired in the UVs for rescue and attack operations in defense applications. A lower pitch angle during constant depth of operation is preferred in UVs as it results into higher comfort and safety. Fig. 14A shows the variation of pitch angle versus time for different buoyancy changes and from these results it can be observed that the pitch angles are almost same for all the buoyancy changes.

These results are achieved because Fig. 14A shows the performance for various buoyancy changes at a constant z_G and final pitching angle is mainly influenced by the stability parameter z_G. Furthermore, a zoomed part for more detailed variation of the pitch angle due to three buoyancy changes is shown in Fig. 14B. From these results it can be observed that even the pitch angle changes with buoyancy. Nevertheless, the changes are small.

Also, the stability analysis of the same design example of the AUV integrated with 2.5 kg buoyancy capacity is investigated for three different z_G as shown in Fig. 14C and Fig. 15. Variation of the pitch angle versus time at different stability parameter z_G in close loop operation is shown in Fig. 14C. Variation of heave velocity versus time is shown in Fig. 15A and Fig. 15B shows the variation of depth versus time at different z_G in closed loop operation.

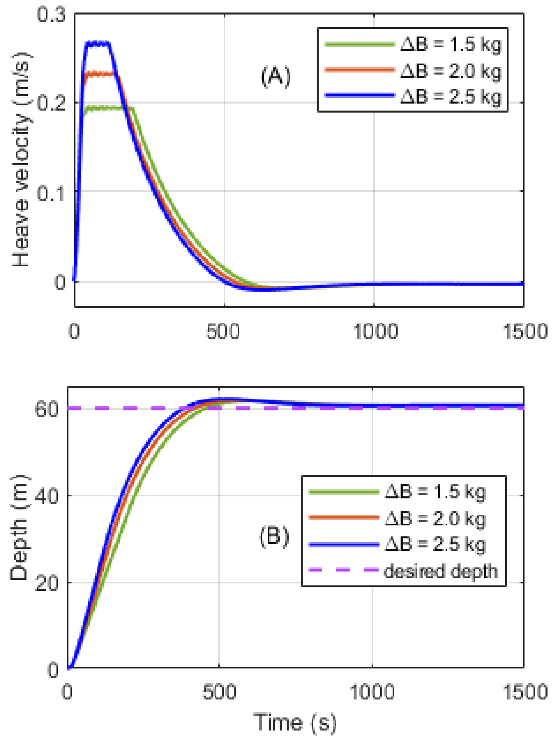

Figure 13: A - Variation of the heave velocity versus time and B - Depth of operation versus time in closed loop condition.

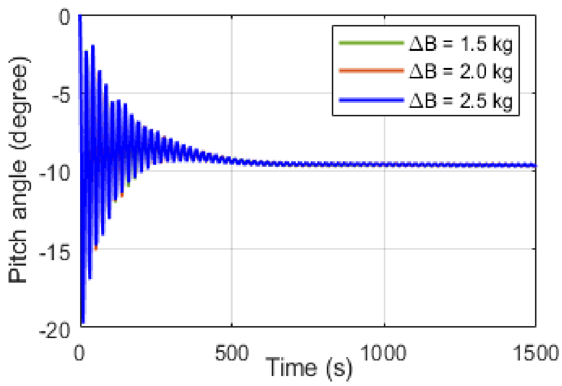

Figure 14: A - Variation of the pitch angle versus time in close loop operation at constant z_G.

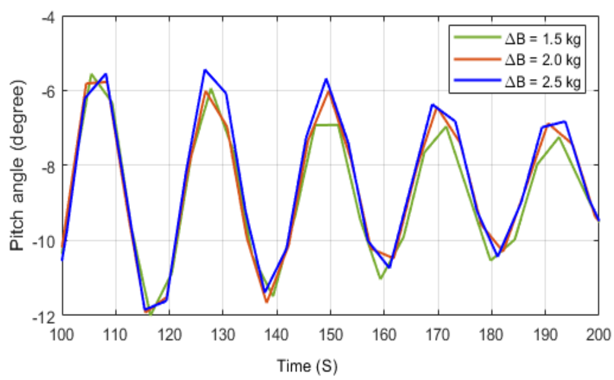

Figure 14: B - Zoomed part of variation of the pitch angle versus time in close loop operation at constant z_G.

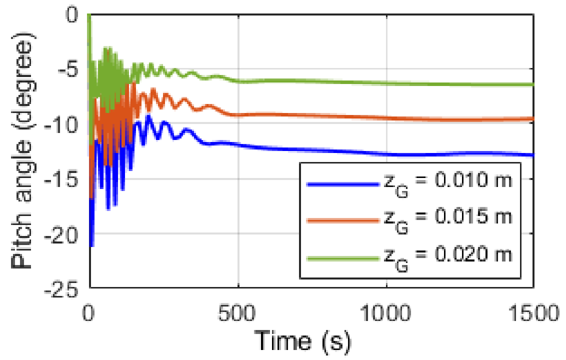

Figure 14: C - Variation of the pitch angle versus time in close loop operation at different z_G

From these results it is observed that the heave velocity and operating depth performances are similar because heave velocity is mainly a function of buoyancy change which is considered constant. However a minor variation is noted on steady error at different z_G. Table 3 shows the steady state error achieved for the heave velocity and depth at various z_G. Additionally, the standard law of stability criteria for better restoring moment of submerged body is a function of the difference between CG and geometric center, for more details see (Chen et al., 2017). With these, the final settling pitch angle decreases with an increase in the z_G. From the results of Fig. 14C, it can be observed that for z_G = 0.010 m, the final settling pitch angle achieved is almost 13 degree and at z_G = 0.020 m the final settling pitch angle is 6.5 degree. These results indicate that the presented simulation results are following the standard stability criteria.

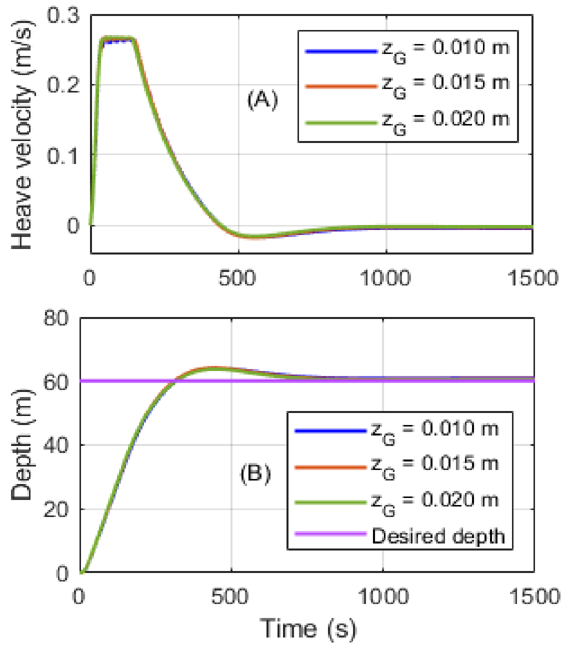

Figure 15: A - Variation of the heave velocity versus time and B - Depth versus time at different z_G in closed loop operation.

Table 3: Steady state error achieved for heave velocity and depth at various z_G.

	Steady State Error	
	Heave velocity (m/s)	Depth (m)
For z_G = 0.010 m	0.004	0.76
For z_G = 0.015 m	0.003	0.55
For z_G = 0.020 m	0.002	0.36

5. CONCLUSIONS

This paper presented the design, development and analysis of VBS integrated with an UV of length of 3.0 m for buoyancy capacity of $\pm\Delta B$ = 5 kg. Performance analyses for the designed VBS in stand-alone mode and in integrated mode with the AUV have been presented for different buoyancy capacities and the results have shown excellent performances.

In the presented results, it has been shown that the targeted depth control of AUV is possible using the state feedback (i.e. LQR controller) and it can be achieved with good performance with almost zero overshoot. Satisfactory performance of the designed and developed VBS were observed in the experimental tests and now it needs to be tested more exhaustively for different depth ratings. Numerical results of the VBS in integration with an AUV needs to be confirmed in-detail with field experiments. Also, it is noted that the present design will need an integration with navigational path planning algorithms (e.g. A^* algorithm), analysis of natural system behaviour and coupling effects to ensure its seamless application in an integrative environment for UVs aimed towards civil and defense applications. Future work shall go in these directions and some of them are currently being investigated.

6. ACKNOWLEDGEMENTS

This research was supported by the internal research grants of IIT madras through research scheme: OE14D212 and from Marine Systems Panel, NRB, India via a sponsored project: NRB-263/MAR/12-13

7. REFERENCES

1. BEYAZAY, B. (1999) *Simulation and Modeling of a Soft Grounding System for an AUV*. MS Thesis, Naval Postgraduate School, Monterey, USA.
2. CHEN, C. W., JIANG, Y., HUANG, H. C., JI, D. X., SUN, G. Q., YU, Z. and CHEN, Y. (2017) *Computational Fluid Dynamics Study of the Motion Stability of an Autonomous Underwater Helicopter*. Ocean Engineering, Vol. 143, pp. 227-239.

3. DOUGLAS, C.W., SIMONETTI, P.J. and JONES, C.P. (2001) *SLOCUM: An Underwater Glider Propelled by Environmental Energy*. IEEE Journal of Oceanic Engineering, Vol. 26 (4), pp. 447–453.
4. DZIELSKI, E., TANGIRALA, C., MOYER, W. W. and BRADLEY, D. L. (2002) *NAVOCEANO Seahorse AUV Design, Testing, and Capabilities*. OCEANS'02 MTS/IEEE, USA, Vol. 1, pp. 151-155, DOI: 10.1109/OCEANS.2002.1193263
5. ERIKSEN, C.C., OSSE, T.J., LIGHT, T., WEN, R.D., LEHMANN, T.W., SABIN, P.L. and BALLARD J.W. (2001) *Long Range Autonomous Underwater Vehicle for Oceanographic Research*. IEEE Journal of Oceanic Engineering, Vol. 26 (4), pp. 424–436.
6. FOSSEN, T.I. (1999) *Guidance and Control of Ocean Vehicle*. John Wiley & Sons, USA.
7. FOSSEN, T.I. (2011) *Handbook of Marine Craft Hydrodynamics and Motion Control*. John Wiley & Sons, USA.
8. HYAKUDOME, T., AOKI, T., MURASHIMA, T., TSUKIOKA, S., YOSHIDA, H., NAKAJOH, H., IDA, T., ISHIBASHI, S. and SASAMOTO, R. (2002) *Key Technologies for AUV URASHIMA*. OCEANS'02 MTS/IEEE, USA, pp. 162–166, DOI: 10.1109/OCEANS.2002.1193265.
9. JENSEN, H.F. (2009) *Variable Buoyancy System Metric*. MS Thesis., Massachusetts Institute of Technology, USA.
10. KATSUHIKO, O. (2010) *Modern Control Engineering*. 9th Ed. Prentice-Hall, USA.
11. MUÑIZ, J.P.O. AND JIMENEZ, T.S. (2018) *VBS Design and Modeling for a Coastal Underwater Glider*. OCEANS'18 MTS/IEEE, USA, pp. 1-7. DOI: 10.1109/OCEANS.2018.8604817
12. RANGANATHAN, T., SINGH, V., NAIR, R. and THONDIYATH, A. (2017) *Design of A Controllable Variable Buoyancy Module and its Performance Analysis as a Cascaded System for Selective Underwater Deployment*. Journal of Engineering for the Maritime Environment, Vol. 231 (4), pp. 888-901.
13. SHERMAN, J., DAVIS, R.E., OWENS, W.B. and VALDES, J. (2001) *The Autonomous Underwater Glider: Spray*. IEEE Journal of Oceanic Engineering, Vol. 26 (4), pp. 437-446.
14. SHIBUYA, K., KISHIMOTO, Y. and YOSHII S. (2013) *Depth Control of Underwater Robot with Metal Bellows Mechanism for Buoyancy Control Device Utilizing Phase Transition*. Journal of Robotics and Mechatronics, Vol. 25 (5), pp. 795-803.
15. SNAME (1950) *Nomenclature for Treating the Motion of a Submerged Body Through a Fluid*. SNAME Technical and Research Bulletin No. 1–5, USA.
16. STEPHEN, B. and CRAIG, B. (1991) *Linear Controller Design-Limits of Performance*. Prentice-Hall, USA.
17. THORLEIFSON, J. M., DAVIES, T. C., BLACK, M. R., HOPKIN, D. A., VERRALL, R. I., POPE, A., MONTEITH, I., DEN H.V. and BUTLER, B. (1997) *The Theseus Autonomous Underwater Vehicle: A Canadian Success Story*. OCEANS' 97 MTS/IEEE, Canada, pp. 1001-1006. DOI: 10.1109/OCEANS.1997.624127
18. TIWARI, B.K. and SHARMA, R. (2018) *A Computing Model for Design of Flexible Buoyancy System for Autonomous Underwater Vehicles and Gliders*. Defence Science Journal, Vol. 68 (6), pp. 589-596.
19. TIWARI, B.K. and SHARMA, R. (2020) *Design and Analysis of a Variable Buoyancy System for Efficient Hovering Control of Underwater Vehicles with State Feedback Controller*. Journal of Marine Science and Engineering, Vol. 8 (263), pp. 1-31.
20. TIWARI, B.K. and SHARMA, R. (2021) *Study on System's Design and Integration for Variable Buoyancy Systems for Underwater Operation.* Defence Science Journal, Vol. 71 (1), pp. 124-133.
21. TIWARI, B.K., SHARMA, R. and ASOKAN, T. (2016) *A Computer Simulation Model for Design of Variable Buoyancy System for Autonomous Underwater Vehicles/Gliders*. OCEANS'16 MTS/IEEE, Shanghai, China, pp. 1-7, DOI: 10.1109/OCEANSAP.2016.7485723.

APPENDIX A: DETAILS ABOUT THE EXPERIMENTS AND COMPARISON

In this study all the numerical simulations are done with fluid assumed to be the sea water as because sea/ocean going UVs are the targeted applications.

Testing in sea/ocean for the stand-alone mode is difficult and prohibitively expensive because of its dependence on boat/ship. In an integrated mode, it will depend upon the AUV and boat/ship. These also will be expensive. But, testing in an integrated mode is the final aim and that will be explored in future.

Table 4: Technical details of the water tank and water properties.

S. No.	Parameter	Value
1	Depth	2.5 m
2	Length * Width	90 m * 4m
3	Water density	1000 kg/m^3
4	Temperature	30 ^{o}C
5	Wave/current	No

Experimental testing is done in the deep water tank and technical details of the tank are listed in Table 4. Tank water is fresh water and its properties are also listed in Table 4. As the water depth available in the tank is 2.5 m only, the testing is restricted to 2.0 m to avoid hard/crash landing on the bottom. In testing three readings (repeat in 3 cycles) are considered and approach is to plot the average values to ensure that the values do not vary more than +/- 5%. In case there is large variation then the experiments are repeated.

Regarding, the experimental testing, the following can be observed from Fig. 6:

- (A) Experimental results agree with the simulation results broadly and the observed differences are noticeable only at 0.5 m and 1.5 m (around 5 s and 9 s) both in sinking phase and rising phase. This is because of multiple reasons, e.g. minor differences in the densities of sea water and fresh water; start of the inflow in tank during sinking and outflow from the tank during rising is slow because the pump stabilizes after some gap; and initial addition/deletion of water up to certain low volume from tanks does not induce sinking or rising because some critical volume is needed to overcome inertia.
- (B) Around 2 s are needed for the system to add/delete critical mass and then the sinking/rising can be observed.
- (C) Initial sinking/rising is slow and then it accelerates and these are expected as it is noted in the explanation given in (A).

